

ManifoldNet: A Deep Network Framework for Manifold-valued Data

Rudrasis Chakraborty[†], Jose Bouza[†], Jonathan Manton⁺ and Baba C. Vemuri^{†*}

[†] Department of CISE, University of Florida, FL 32611, USA
 {rudrasischa, baba.vemuri}@gmail.com, josebouza@ufl.edu,
 jonathan.manton@ieee.org

Abstract

Deep neural networks have become the main work horse for many tasks involving learning from data in a variety of applications in Science and Engineering. Traditionally, the input to these networks lie in a vector space and the operations employed within the network are well defined on vector-spaces. In the recent past, due to technological advances in sensing, it has become possible to acquire manifold-valued data sets either directly or indirectly. Examples include but are not limited to data from omnidirectional cameras on automobiles, drones etc., synthetic aperture radar imaging, diffusion magnetic resonance imaging, elastography and conductance imaging in the Medical Imaging domain and others. Thus, there is need to generalize the deep neural networks to cope with input data that reside on curved manifolds where vector space operations are not naturally admissible. In this paper, we present a novel theoretical framework to generalize the widely popular convolutional neural networks (CNNs) to manifold-valued data inputs. We call these networks, ManifoldNets.

In ManifoldNets, convolution operation on data residing on Riemannian manifolds is achieved via a provably convergent recursive computation of the weighted Fréchet Mean (wFM) of the given data, where the weights makeup the convolution mask, to be learned. Further, we prove that the proposed wFM layer achieves a contraction mapping and hence ManifoldNet does not need the additional non-linear ReLU unit used in standard CNNs. Operations such as pooling in traditional CNN are no longer necessary in this setting since wFM is already a pooling type operation. *Analogous to the equivariance of convolution operation in Euclidean space to translations, we prove that the wFM is equivariant to the action of the group of isometries admitted by the Riemannian manifold on which the*

*This research was funded in part by the NSF grant IIS-1525431 and IIS-1724174 to BCV.

data reside. This equivariance property facilitates weight sharing within the network. We present experiments, using the ManifoldNet framework, to achieve video classification and image reconstruction using an auto-encoder+decoder setting. Experimental results demonstrate the efficacy of ManifoldNets in the context of classification and reconstruction accuracy.

1 Introduction

Convolutional neural networks (CNNs) have attracted enormous attention in the past decade due to their significant success in Computer Vision, Speech Analysis and other fields. CNNs were pioneered by Lecun in [32] and gained much popularity ever since their significant success on Imagenet data reported in Krizhevsky et al. [31]. Most of the deep networks and in particular CNNs have traditionally been restricted to dealing with data residing in vector spaces. However, in the past few years, there is growing interest in generalizing the CNNs and deep networks in general to data that reside in non-Euclidean spaces and possibly on smooth manifolds. In this context, at the outset, it would be useful to categorize problems into those that involve data as samples of real-valued functions defined on a manifold and those that are simply manifold-valued and hence are sample points on a manifold.

In the context of input data being samples of functions on smooth manifolds, recently there has been a flurry of activity in developing methods that can cope specifically with samples of functions on a sphere i.e., spherical functions that are encountered in many applications such as, omnidirectional cameras on drones, robots etc., meteorological data and many others. The key property that allows learned weight sharing in CNNs is the equivariance to translations. The simplest technique to achieve equi-variance is via data augmentation [31, 14]. Cascade of wavelet transforms to achieve equivariance was shown in [6, 39]. In [18], authors describe ‘Symnet’, which achieves invariance to symmetry group actions. Equivariance to discrete group actions was achieved through parameter sharing in [40]. For the case of data on a spherical domain, one considers exploiting equivariance to the natural symmetry group operation on the sphere, which is the rotation group. Several research groups recently reported spherical-CNNs (SCNNs) to accommodate such an equivariance in defining the convolution of functions [46, 11, 12]. In another recent work [17], authors describe a polar transformer network, which is equivariant to rotations and scaling transformations. By combining this with what is known in literature as a spatial transformer [26], they achieve equivariance to translations as well. More generally, equivariance of convolution operations to group actions admitted by the domain manifold is what is needed to this end and most recent work reported in [9, 30] achieves this for homogeneous Riemannian manifolds, which are more general than Lie groups.

In this paper we will consider the second problem, namely, when the input data are sample points on known Riemannian manifolds for example, the manifold of symmetric positive definite matrices, P_n , the special orthogonal group, $SO(n)$,

the n-sphere, \mathbf{S}^n , the Grassmannian, $\text{Gr}(p, n)$, and others. There is very little prior work that we are aware of on deep networks that can cope with input data samples residing on these manifolds with the exception of [25, 24]. In [25], authors presented a deep network architecture for classification of hand-crafted features residing on a Grassmann manifold that form the input to the network. Their network architecture contains 3 blocks, the first block involves a full rank mapping (to be learned) of the input orthonormal matrices followed by re-orthonormalization operation achieved via the well known QR -decomposition followed by the well known projection operation involving a projection metric on the Grassmannian. The second block consists of a pooling block which involves computing the arithmetic mean that is valid since the projection matrices lie in a Euclidean space. The third block is a standard fully connected layer with softmax operations whose output is amenable to classification. In [24], authors present a deep network architecture for data residing on P_n . They proposed three types of layers in the architecture. The first involves a bilinear mapping of the input SPD matrices on P_n to the SPD matrices on P_{n+1} . The second type of layer is supposed to mimic the ReLU type operation which is achieved by using the ‘max’ between the scaled identity and the true diagonal eigen-value matrix in order to reconstruct a new SPD matrix from the input SPD matrix to this nonlinear ReLU type operation. Finally, they use the Log-Euclidean framework described in [2] which maps points on P_n into the tangent space of P_n by using the Riemannian *Log* map [15] and then uses the standard Euclidean computations since the tangent space is isomorphic to the Euclidean space. This layer is then followed by a fully connected layer and softmax operations as in the conventional CNNs. Note that in both these works, the architecture does not introduce any convolution or equivalent operations on the Grassmannian or P_n . Further, it does not use the natural invariant metric on the Grassmannian or P_n , nor does it use intrinsic operations on these manifolds in the blocks. Using intrinsic operations within the layers guarantees that the result remains on the manifold and hence does not require any projection (extrinsic) operations to ensure the result lies in the same space. Such extrinsic operations are known to yield results that are susceptible to significant inaccuracies when the data variance is large. For example, the Fréchet mean when computed using the Log-Euclidean metric – which is an extrinsic metric – proves to be inaccurate compared to the intrinsic mean when data variance is large as was demonstrated in [41]. Since there is no operation analogous to a convolution on these manifolds in their network, it does not yield a natural generalization to the CNN and does not have any equivariance property to the action of group of isometries admitted by the manifold.

There are several deep networks reported in literature to deal with cases when data reside on 2-manifolds encountered in Computer Vision and Graphics for modeling shapes of objects. Some of these are based on graph-based representations of points on the surfaces in 3D and a generalization of CNNs to graphs [22, 13]. There is also recent work in [35] where the authors presented a deep network called geodesic CNN (GCNN), where convolutions are performed in local geodesic polar charts constructed on the manifold. For more literature

on deep networks for data on 2-manifolds, we refer the interested reader to a recent survey paper [5] and references therein.

In this paper, we present a novel deep learning framework called Manifold-Nets. These are the analogues of CNNs and can handle input data residing on Riemannian manifolds. Our key contributions in this work are: (i) we define the convolution operation on the manifold to be one of estimating the weighted Fréchet mean (wFM) for which we present a provably convergent, efficient and recursive estimator. In [19], authors observed that convolution of functions defined on the unit Hilbert sphere can be formulated as a problem involving estimation of the wFM. However, this is distinct from our problem at hand here namely, we are not concerned with functions on the manifold but manifold-valued functions and hence points on the manifold. (ii) A proof of equivariance of wFM to the action of group of isometries admitted by the Riemannian manifold on which the data reside. This equivariance allows the network to share weights within the layers. (iii) A novel deep architecture involving the Riemannian counterparts to the conventional CNN units. (iv) Proof of concept experiments demonstrating the performance of the ManifoldNet.

Rest of the paper is organized as follows. In section 2 we present the main theoretical result showing the equivariance of wFM to group actions admitted by the Riemannian manifold. Section 2 also contains a detailed description of the proposed network architecture. In section 3 we present the experimental results and conclude in section 4.

2 Convolution neural network on a Riemannian manifold

In this section, we will define a convolution operation on Riemannian manifolds. Before formally defining the convolution operation and building the convolution neural network for the manifold-valued data, dubbed as ManifoldNet, we first present some relevant concepts from differential geometry that will be used in the rest of the paper.

Preliminaries. Let $(\mathcal{M}, g^{\mathcal{M}})$ be an orientable complete Riemannian manifold with a Riemannian metric $g^{\mathcal{M}}$, i.e., $(\forall x \in \mathcal{M}) g_x^{\mathcal{M}} : T_x\mathcal{M} \times T_x\mathcal{M} \rightarrow \mathbf{R}$ is a bi-linear symmetric positive definite map, where $T_x\mathcal{M}$ is the tangent space of \mathcal{M} at $x \in \mathcal{M}$. Let $d : \mathcal{M} \times \mathcal{M} \rightarrow [0, \infty)$ be the metric (distance) induced by the Riemannian metric $g^{\mathcal{M}}$. With a slight abuse of notation we will denote a Riemannian manifold $(\mathcal{M}, g^{\mathcal{M}})$ by \mathcal{M} unless specified otherwise. Let Δ be the supremum of the sectional curvatures of \mathcal{M} .

Definition 1. Let $p \in \mathcal{M}$ and $r > 0$. Define $\mathcal{B}_r(p) = \{q \in \mathcal{M} | d(p, q) < r\}$ to be an open ball at p of radius r .

Definition 2. [20] Let $p \in \mathcal{M}$. The local injectivity radius at p , $r_{inj}(p)$, is defined as $r_{inj}(p) = \sup \{r | Exp_p : (\mathcal{B}_r(\mathbf{0}) \subset T_p\mathcal{M}) \rightarrow \mathcal{M}$ is defined and is a diffeomorphism

onto its image}. The injectivity radius [34] of \mathcal{M} is defined as $r_{\text{inj}}(\mathcal{M}) = \inf_{p \in \mathcal{M}} \{r_{\text{inj}}(p)\}$.

Within $\mathcal{B}_r(p)$, where $r \leq r_{\text{inj}}(\mathcal{M})$, the mapping $\text{Exp}_p^{-1} : \mathcal{B}_r(p) \rightarrow \mathcal{U} \subset T_p\mathcal{M}$, is called the inverse Exponential/ Log map.

Definition 3. [27] An open ball $\mathcal{B}_r(p)$ is a regular geodesic ball if $r < r_{\text{inj}}(p)$ and $r < \pi / (2\Delta^{1/2})$.

In Definition 3 and below, we interpret $1/\Delta^{1/2}$ as ∞ if $\Delta \leq 0$. It is well known that, if p and q are two points in a regular geodesic ball $\mathcal{B}_r(p)$, then they are joined by a unique geodesic within $\mathcal{B}_r(p)$ [27].

Definition 4. [10] $\mathcal{U} \subset \mathcal{M}$ is strongly convex if for all $p, q \in \mathcal{U}$, there exists a unique length minimizing geodesic segment between p and q and the geodesic segment lies entirely in \mathcal{U} .

Definition 5. [20] Let $p \in \mathcal{M}$. The local convexity radius at p , $r_{\text{cvx}}(p)$, is defined as $r_{\text{cvx}}(p) = \sup \{r \leq r_{\text{inj}}(p) | \mathcal{B}_r(p) \text{ is strongly convex}\}$. The convexity radius of \mathcal{M} is defined as $r_{\text{cvx}}(\mathcal{M}) = \inf_{p \in \mathcal{M}} \{r_{\text{cvx}}(p)\}$.

For the rest of the paper, we will assume that the samples on \mathcal{M} lie inside an open ball $U = \mathcal{B}_r(p)$ where $r = \min \{r_{\text{cvx}}(\mathcal{M}), r_{\text{inj}}(\mathcal{M})\}$, for some $p \in \mathcal{M}$, unless mentioned otherwise. Now, we are ready to define the operations necessary to develop the ManifoldNet.

2.1 Convolution operation on \mathcal{M}

Let $\{X_i\}_{i=1}^N$ be the manifold-valued samples on \mathcal{M} . We define the convolution operation on \mathcal{M} as the weighted Fréchet mean (wFM) [36] of the samples $\{X_i\}_{i=1}^N$. By the aforementioned condition on the samples, the existence and uniqueness of FM is guaranteed [1]. Let $\{w_i\}_{i=1}^N$ be the weights such that they satisfy the convexity constraint, i.e., $\forall i, w_i > 0$ and $\sum_i w_i = 1$, then wFM, $\text{wFM}(\{X_i\}, \{w_i\})$ is defined as:

$$\text{wFM}(\{X_i\}, \{w_i\}) = \underset{M \in \mathcal{M}}{\text{argmin}} \sum_{i=1}^N w_i d^2(X_i, M) \quad (1)$$

For the equivariance property of the convolution, we will show that the convolution is equivariant under the action of the group of isometries of \mathcal{M} . We will first formally define the group of isometries of \mathcal{M} (let us denote it by G) and then define the equivariance property and show that wFM is G -equivariant.

Definition 6 (Group of isometries of \mathcal{M}). A diffeomorphism $\phi : \mathcal{M} \rightarrow \mathcal{M}$ is an isometry if it preserves distance, i.e., $d(\phi(x), \phi(y)) = d(x, y)$. The set $I(\mathcal{M})$ of all isometries of \mathcal{M} forms a group with respect to function composition. Rather than write an isometry as a function ϕ , we will write it as a group action. Henceforth, let G denote the group $I(\mathcal{M})$, and for $g \in G$, and $x \in \mathcal{M}$, let $g.x$ denote the result of applying the isometry g to point x .

Clearly \mathcal{M} is a G set (see [16] for definition of a G set). We will now define equivariance and show that wFM, i.e., the convolution operator, is G -equivariant.

Definition 7 (Equivariance). *Let X and Y be G sets. Then, $F : X \rightarrow Y$ is said to be G -equivariant if*

$$F(g.x) = g.F(x) \quad (2)$$

for all $g \in G$ and all $x \in X$.

Let $U \subset \mathcal{M}$ be an open ball inside which FM exists and is unique, let P be the set consists of all possible finite subsets of U .

Theorem 1. *Given $\{w_i\}$ satisfying the convex constraint, let $F : P \rightarrow U$ be a function defined by $\{X_i\} \mapsto \text{wFM}(\{X_i\}, \{w_i\})$. Then, F is G -equivariant.*

Proof. Let $g \in G$ and $\{X_i\}_{i=1}^N \in P$, now, let $M^* = \text{wFM}(\{X_i\}, \{w_i\})$, as $g.F(\{X_i\}) = g.M^*$, it suffices to show $g.M^*$ is $\text{wFM}(\{g.X_i\}, \{w_i\})$ (assuming the existence and uniqueness of $\text{wFM}(\{g.X_i\}, \{w_i\})$ which is stated in the following claim).

Claim: Let $U = \mathcal{B}_r(p)$ for some $r > 0$ and $p \in \mathcal{M}$. Then, $\{g.X_i\} \subset \mathcal{B}_r(g.p)$ and hence $\text{wFM}(\{g.X_i\}, \{w_i\})$ exists and is unique.

Let \widetilde{M} be $\text{wFM}(\{g.X_i\}, \{w_i\})$. Then,

$$\sum_{i=1}^N w_i d^2(g.X_i, \widetilde{M}) = \sum_{i=1}^N w_i d^2(X_i, g^{-1}.\widetilde{M})$$

Since, $M^* = \text{wFM}(\{X_i\}, \{w_i\})$, hence, $M^* = g^{-1}.\widetilde{M}$, i.e., $\widetilde{M} = g.M^*$. Thus, $g.M^* = \text{wFM}(\{g.X_i\}, \{w_i\})$, which implies F is G -equivariant. \blacksquare

Now we give some examples of \mathcal{M} with the corresponding group of isometries G . Let $\mathcal{M} = \text{SPD}(n)$ (the space of $n \times n$ symmetric positive-definite matrices). Let d be the Stein metric on $\text{SPD}(n)$. Then, the group of isometries G is $\text{O}(n)$ (the space of $n \times n$ orthogonal matrices). A class of Riemannian manifolds on which G acts transitively are called Riemannian homogeneous spaces. We can see that on a Riemannian homogeneous space \mathcal{M} , wFM is G -equivariant. Equipped with a G -equivariant operator on \mathcal{M} , we can claim that the wFM (defined above) is a valid convolution operator since group equivariance is a unique defining property of a convolution operator. The rest of this subsection will be devoted to developing an efficient way to compute wFM. Let $\omega^{\mathcal{M}} > 0$ be the Riemannian volume form. Let $p_{\mathbf{X}}$ be the probability density of a U -valued random variable \mathbf{X} with respect to $\omega^{\mathcal{M}}$ on $U \subset \mathcal{M}$, so that $\Pr(X \in \mathfrak{A}) = \int_{\mathfrak{A}} p_{\mathbf{X}}(Y) \omega^{\mathcal{M}}(Y)$ for any Borel-measurable subset \mathfrak{A} of U . Let $Y \in U$, we can define the expectation of the real valued random variable $d^2(\cdot, Y) : U \rightarrow \mathbf{R}$ by $E[d^2(\cdot, Y)] = \int_U d^2(X, Y) p_{\mathbf{X}}(X) \omega^{\mathcal{M}}(X)$. Now, let $w : U \rightarrow (0, \infty)$ be an integrable function and $\int_U w(X) \omega^{\mathcal{M}}(X) = 1$.

Then, observe that,

$$\begin{aligned}
E_w [d^2(\cdot, Y)] &:= \int_U w(X) d^2(X, Y) p_X(X) \omega^{\mathcal{M}}(X) \\
&= C \int_U d^2(X, Y) \tilde{p}_X(X) \omega^{\mathcal{M}}(X) \\
&= C \tilde{E} [d^2(\cdot, Y)].
\end{aligned} \tag{3}$$

Here, \tilde{p}_X is the probability density corresponding to the probability measure $\tilde{\Pr}$ defined by, $\tilde{\Pr}(X \in \mathfrak{X}) = \int_{\mathfrak{X}} \tilde{p}_X(Y) \omega^{\mathcal{M}}(Y) := \int_{\mathfrak{X}} \frac{1}{C} p_X(Y) w(Y) \omega^{\mathcal{M}}(Y)$, where, \mathfrak{X} lies in the Borel σ -algebra over U and $C = \int_U p_X(Y) w(Y) \omega^{\mathcal{M}}(Y)$. Note that the constant $C > 0$, since p_X is a probability density, $w > 0$ and \mathcal{M} is orientable. Thus, $E_w [d^2(\cdot, Y)]$ with respect to p_X is proportional to $\tilde{E} [d^2(\cdot, Y)]$ with respect to \tilde{p}_X .

Now, we will prove that the support of p_X is same as \tilde{p}_X .

Proposition 2. $\text{supp}(p_X) = \text{supp}(\tilde{p}_X)$.

Proof. Let $X \in \text{supp}(p_X)$, then, $p_X(X) > 0$. Since, $w(X) > 0$, hence, $\tilde{p}_X(X) > 0$ and thus, $X \in \text{supp}(\tilde{p}_X)$. On the other hand, assume \tilde{X} to be a sample drawn from \tilde{p}_X . Then, either $p_X(\tilde{X}) = 0$ or $p_X(\tilde{X}) > 0$. If, $p_X(\tilde{X}) = 0$, then, $\tilde{p}_X(\tilde{X}) = 0$ which contradicts our assumption. Hence, $p_X(\tilde{X}) > 0$, i.e., $\tilde{X} \in \text{supp}(p_X)$. This concludes the proof. ■

Proposition 3. $wFE(X, w) = FE(\tilde{X})$

Proof. Let X and \tilde{X} be the \mathcal{M} valued random variable following p_X and \tilde{p}_X respectively. We define the weighted Fréchet expectation (wFE) of X as:

$$wFE(X, w) = \underset{Y \in \mathcal{M}}{\text{argmin}} \int_{\mathcal{M}} w(X) d^2(X, Y) p_X(X) \omega^{\mathcal{M}}(X)$$

Using (3), we get $FE(\tilde{X}) = wFE(X, w)$, as C is independent of the choice of Y , which concludes the proof. ■

Let $\{X_i\}_{i=1}^N$ be samples drawn from p_X and $\{\tilde{X}_i\}_{i=1}^N$ be samples drawn from \tilde{p}_X . In order to compute wFM, we will now present an online algorithm (inductive FM Estimator – dubbed iFME). Given, $\{X_i\}_{i=1}^N \subset U$ and $\{w_i := w(X_i)\}_{i=1}^N$ such that $\forall i, w_i > 0$, the n^{th} estimate, M_n of wFM($\{X_i\}, \{w_i\}$) is given by the following recursion:

$$M_1 = X_1 \quad M_n = \Gamma_{M_{n-1}}^{X_n} \left(\frac{w_n}{\sum_{j=1}^n w_j} \right). \tag{4}$$

In the above equation, $\Gamma_X^Y : [0, 1] \rightarrow U$ is the shortest geodesic curve from X to Y . Observe that, in general wFM is defined with $\sum_{i=1}^N w_i = 1$, but in above definition, $\sum_{i=1}^N w_i \neq 1$. We can normalize $\{w_i\}$ to get $\{\tilde{w}_i\}$ by $\tilde{w}_i = w_i / (\sum_i w_i)$, but then Eq. 4 will not change as $\tilde{w}_n / (\sum_{j=1}^n \tilde{w}_j) = w_n / (\sum_{j=1}^n w_j)$. This gives us an efficient inductive/recursive way to define convolution operation on \mathcal{M} . Now, we state and prove that the proposed wFM estimator is consistent.

Proposition 4. *Using the above notations and assumptions, let $\{X_i\}_{i=1}^N$ be i.i.d. samples drawn from p_X on \mathcal{M} . Let the wFE be finite. Then, M_N converges a.s. to wFE as $N \rightarrow \infty$.*

Proof. Using Proposition 3, we know that $\exists \tilde{p}_X$ such that, $\text{wFE}(X, w) = \text{FE}(\tilde{X})$. Thus, it is enough to show the consistency of our proposed estimator when weights are uniform. In order to prove the consistency, we will split the proof into two cases namely, manifolds with (i) non-positive sectional curvature and (ii) non-negative sectional curvature. The reason for doing this split is so that we can use existing theorems in literature for proving the result. We will use the theorems proved in [43] and [4] for manifolds with non-positive and non-negative sectional curvatures respectively. Note that the proof holds only for manifolds with a uniform sign of sectional curvatures.

Theorem 5 (\mathcal{M} has non-negative sectional curvature). *Using the above notations, if $\exists A > 0$ such that, $d(M_n, X_{n+1}) \leq A$ for all n . Then, M_N converges a.s. to wFE as $N \rightarrow \infty$ (see [4] for the proof).*

Theorem 6 (\mathcal{M} has non-positive sectional curvature). *Using the above notations M_N converges a.s. to wFE as $N \rightarrow \infty$ (see [43] for the proof).*

■

2.2 Nonlinear operation between convolutional layers for \mathcal{M} -valued Data

In the traditional CNN model, we need a nonlinear function between two convolutional layers similar to ReLU and softmax. As argued in [33], any nonlinear function used in CNN is basically a contraction mapping. Formally, let F be a nonlinear mapping from U to V . Let assume, U and V are metric spaces equipped with metric d_U and d_V respectively. Then, F is a contraction mapping iff $\exists c < 1$ such that,

$$d_V(F(x), F(y)) \leq c d_U(x, y) \quad (5)$$

F is a non-expansive mapping [33] iff

$$d_V(F(x), F(y)) \leq d_U(x, y) \quad (6)$$

One can easily see that the popular choices for nonlinear operations like ReLU, sigmoid are in fact non-expansive mappings. Now, we will show that the

function wFM as defined in 1, is a contraction mapping for non-trivial choices of weights. Let $\{X_i\}_{i=1}^N$ and $\{Y_j\}_{j=1}^M$ be the two set of samples on \mathcal{M} . Without any loss of generality, assume $N \leq M$. We consider the set $\mathcal{U}^M = \underbrace{U \times \dots \times U}_{M \text{ times}}$.

Clearly $\{Y_j\}_{j=1}^M \in \mathcal{U}^M$ and we embed $\{X_i\}_{i=1}^N$ in \mathcal{U}^M as follows: we construct $\{\tilde{X}_i\}_{i=1}^M$ from $\{X_i\}_{i=1}^N$ by defining $\tilde{X}_i = X_{(i-1) \bmod N + 1}$. Let us denote the embedding by ι . Now, define the distance on \mathcal{U}^M as follows:

$$d\left(\{\tilde{X}_i\}_{i=1}^M, \{Y_j\}_{j=1}^M\right) = \max_{i,j} d(X_i, Y_j) \quad (7)$$

We will say the choice of weights for wFM is trivial if one of the weights is 1 and hence the rest are 0.

Proposition 7. *For all nontrivial choices of $\{\alpha_i\}_{i=1}^N$ and $\{\beta_j\}_{j=1}^M$ satisfying the convexity constraint, $\exists c < 1$ such that,*

$$d\left(\text{wFM}\left(\{X_i\}_{i=1}^N, \{\alpha_i\}_{i=1}^N\right), \text{wFM}\left(\{Y_j\}_{j=1}^M, \{\beta_j\}_{j=1}^M\right)\right) \leq c d\left(\iota\left(\{X_i\}_{i=1}^N\right), \{Y_j\}_{j=1}^M\right) \quad (8)$$

Proof. This is easy to prove and hence we skip the proof here. ■

2.3 The invariant (last) layer

We will form a convolution network by cascading multiple wFM blocks each of which acts as a convolution layer. Each convolutional layer is equivariant to the group operation, and hence at the end of the cascaded convolutional layers, the output is equivariant to the group action applied to the input of the network. Let d be the number of output channels each of which outputs a wFM, hence each of the channels is equivariant to the group action. However, in order to build a network that yields an output which is invariant to the group action, we now seek the last layer (i.e., the linear classifier) to be invariant to the group action. The last layer is thus constructed as follows: Let $\{Z_1, \dots, Z_d\} \subset \mathcal{M}$ be the output of d channels and $M_u = \text{FM}\left(\{Z_i\}_{i=1}^d\right) = \text{wFM}\left(\{Z_i\}_{i=1}^d, \{1/d\}_1^d\right)$ be the unweighted FM of the outputs $\{Z_i\}_{i=1}^d$. Then, we construct a layer with d outputs whose i^{th} output $o_i = d(M_u, Z_i)$. Let c be the number of classes for the classification task, then, a fully connected (FC) layer with inputs $\{o_i\}$ and c output nodes is build. A softmax operation is then used at the c output nodes to obtain the outputs $\{y_i\}_{i=1}^c$. In the following proposition we claim that this last layer with $\{Z_i\}_{i=1}^d$ inputs and $\{y_i\}_{i=1}^c$ outputs is group invariant.

Proposition 8. *The last layer with $\{Z_i\}_{i=1}^d$ inputs and $\{y_i\}_{i=1}^c$ outputs is group invariant.*

Proof. Using the above construction, let $W \in \mathbf{R}^{c \times d}$ and $\mathbf{b} \in \mathbf{R}^c$ be the weight matrix and bias respectively of the FC layer. Then,

$$\begin{aligned} \mathbf{y} &= F(W^T \mathbf{o} + \mathbf{b}) \\ &= F(W^T d(M_u, Z) + \mathbf{b}), \end{aligned} \quad (9)$$

where, F is the softmax function. In the above equation, we treat $d(M_u, Z)$ as the vector $[d(M_u, Z_1), \dots, d(M_u, Z_d)]^t$. Observe that, $g.M_u = \text{FM}(\{g.Z_i\}_{i=1}^d)$. As each of the d channels is group equivariant, Z_i becomes $g.Z_i$. Because of the property of the distance under group action, $d(g.M_u, g.Z_i) = d(M_u, Z_i)$. Hence, one can see that if we change the inputs $\{Z_i\}$ to $\{g.Z_i\}$, the output \mathbf{y} will remain invariant. ■

In Fig. 1 we present a schematic of ManifoldNet depicting the different layers of processing the manifold-valued data as described above in Sections 2.1-2.3.

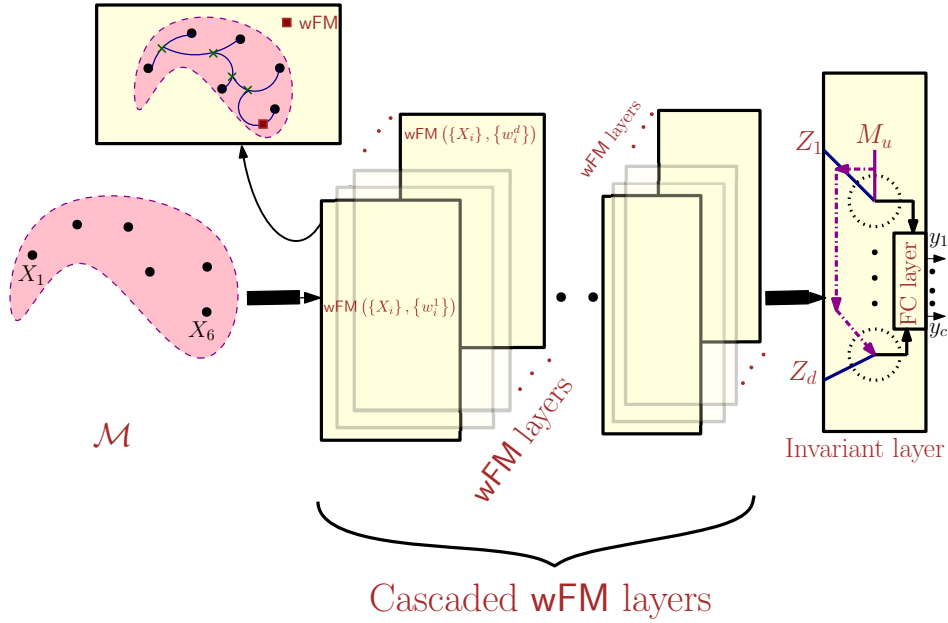


Figure 1: Schematic diagram of ManifoldNet

3 Experiments

In this section we present performance of the ManifoldNet framework on several computer vision problems. The breadth of application coverage here includes classification and reconstruction problems. We begin with a video classification problem and then present a reconstruction problem using an auto-encoder-decoder set up.

3.1 Video Classification

We start by using the method in [48] which we summarize here. Given a video with dimensions $F \times 3 \times H \times W$ of F frames, 3 color channels and a frame size of $H \times W$, we can apply a convolution layer to obtain an output of size $F \times C \times H' \times W'$ consisting of C channels of size $H' \times W'$. Interpreting each channel as a feature map, we shift the features to have a zero mean and compute the covariance matrix of the convolution output to obtain a sequence of F symmetric positive (semi) definite (SPD) matrices of size $C \times C$. From here we can apply a series of temporal ManifoldNet convolutions (i.e. weighted FM's) to transform the $F \times C \times C$ input to a temporally shorter $F' \times K \times C \times C$ output, where K are the temporal convolution channels. Within the temporal ManifoldNet convolutions we use a simple weight normalization to ensure that the weights are within $[0, 1]$, and for the weights w_i of any output channel we add a weight penalty of the form $(\sum w_i - 1)^2$ to the loss function to ensure that we obtain a proper wFM. We then reshape this to $F'K \times C \times C$ and pass it through an invariant final layer (section 2.3) to obtain a vector of size $F'K$. Finally, a single FC+SoftMax layer is applied to produce a classification output. We call this the SPD temporal convolutional architecture SPD-TCN. Figure 3.1 illustrates the network architecture described above. In general, the SPD-TCN tends to perform very well on video classification tasks while using very few parameters, and runs efficiently due to the convolutional structure.

We tested the ManifoldTCN on the Moving MNIST dataset [42]. In [8] authors developed a manifold valued recurrent network architecture, dubbed as SPD-SRU, which produced state of the art classification results on a version of the Moving MNIST dataset in comparison to LSTM [23], SRU [37], TT-LSTM and TT-GRU [47] networks. For the LSTM and SRU networks, convolution layers are also used before the recurrent unit. We will compare directly with these results. For details of the various architectures used please see section 5 of [8]. The Moving MNIST data generated in [42] consists of 1000 samples, each of 20 frames. Each sample shows two randomly chosen MNIST digits moving within a 64×64 frame, with the direction and speed of movement fixed across all samples in a class. The speed is kept the same across different classes, but the digit orientation will differ across two different classes. We summarize the 10-fold cross validation results for several orientation differences between classes in Table 3.1. For this experiment the SPD-TCN will consist of a single convolution layer with kernel size 5 and stride 3 returning 8 channels, making for an 8×8 covariance matrix. We then apply three temporal SPD convolution layers of kernel size 3 and stride 2, with the following channels $1 \rightarrow 4 \rightarrow 8 \rightarrow 16$, i.e. after these three temporal SPD convolutions we have 16 temporal channels. This $16 \times 8 \times 8$ is used as an input to the invariant final layer to get a 16 dimensional output vector, which is transformed by a fully connected layer and SoftMax to obtain the output.

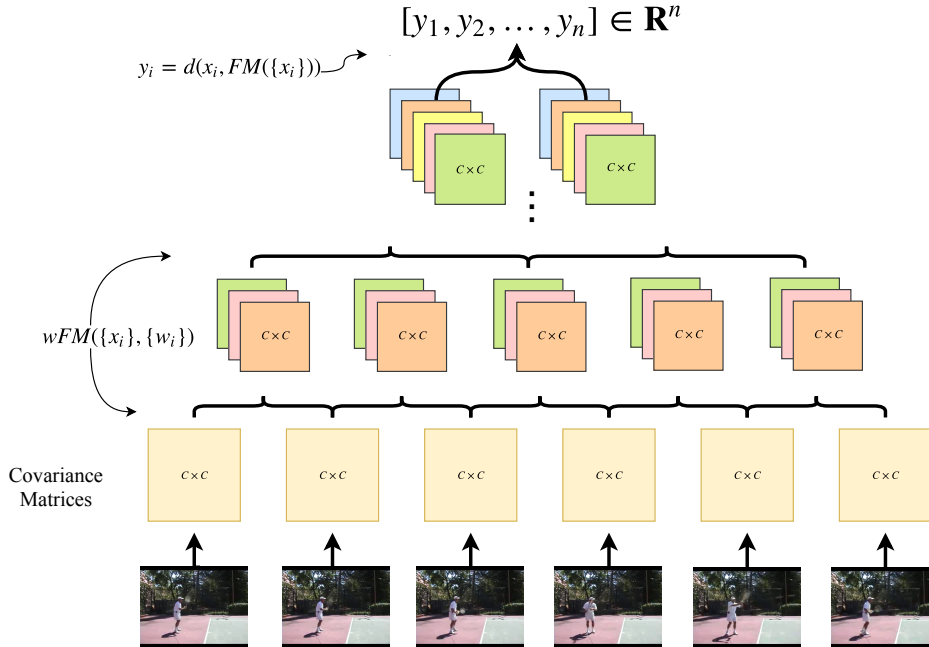


Figure 2: ManifoldTCN Network Architecture

Mode	# params.	time (s) / epoch	orientation ($^{\circ}$)		
			30-60	10-15	10-15-20
SPD-TCN	738	~ 2.7	1.00 ± 0.00	0.99 ± 0.01	0.97 ± 0.02
SPD-SRU	1559	~ 6.2	1.00 ± 0.00	0.96 ± 0.02	0.94 ± 0.02
TT-GRU	2240	~ 2.0	1.00 ± 0.00	0.52 ± 0.04	0.47 ± 0.03
TT-LSTM	2304	~ 2.0	1.00 ± 0.00	0.51 ± 0.04	0.37 ± 0.02
SRU	159862	~ 3.5	1.00 ± 0.00	0.75 ± 0.19	0.73 ± 0.14
LSTM	252342	~ 4.5	0.97 ± 0.01	0.71 ± 0.07	0.57 ± 0.13

Table 1: Comparison results on Moving MNIST

3.2 Dimensionality Reduction

Here we present experiments demonstrating the applicability of the theory laid out in Section 2 to the case of linear dimensionality reduction, specifically principal component analysis (PCA), which is the workhorse of many machine learning algorithms. In [7], authors presented an online subspace averaging algorithm for construction of principal components via intrinsic averaging on the Grassman-

nian. In this section, we achieve the intrinsic Grassmann averaging process in the framework of ManifoldNets to compute the principal subspaces and achieve the dimensionality reduction. In the context of deep neural networks, dimensionality reduction is commonly achieved via an autoencoder architecture. More recently, deep neural networks have shown promising results when the data manifold is intrinsically non-linear, as in the case of natural images. In the deep learning community this has become a field in its own right, known as representation learning or feature learning [3]. This field has seen several significant advances in the past few years, including the introduction of denoising autoencoders [45], variational autoencoders [29], autoregressive models (PixelCNN [38], PixelRNN [44]), and flow-based generative models [28]. Many of these architectures are modifications of the traditional autoencoder network, which involves learning an identity map through a small latent space. In our application, we modify the traditional autoencoder model by adding a ManifoldNet layer to perform a learned linear dimensionality reduction in the latent space, although in principal, our techniques can be applied to most autoencoder based models such as the variational autoencoders.

To compute a linear subspace in the ManifoldNet framework we use an intrinsic averaging scheme on the Grassmannian. Points on the Grassmannian $\text{Gr}(k, n)$ correspond to k -dimensional subspaces of the vector space \mathbf{R}^n . The Grassmannian is a smooth homogeneous manifold and points $\mathcal{X} \in \text{Gr}(k, n)$ on the Grassmannian can be specified by an orthonormal basis X , i.e. an $n \times k$ orthonormal matrix. Hauberg et al. showed that the one dimensional principal subspace can be computed as an average of all one dimensional subspaces spanned by normally distributed data [21]. Motivated by this result, Chakraborty et al. proposed an efficient intrinsic averaging scheme on $\text{Gr}(k, n)$ that converges to the k -dimensional principal subspace of a normally distributed dataset in \mathbf{R}^n [7]. In the ManifoldNet framework we can modify this technique to learn a weighted FM of points on the Grassmannian that corresponds to a subspace of the latent space which minimizes the reconstruction error by using a Grassmannian averaging layer that learns the weights in the wFM. This essentially will give us a lower dimensional representation of the samples after projecting them on to the learned subspace. Note that combining the convergence proof in Chakraborty et al. [7] and Proposition 3, we claim that the wFM learned using the ManifoldNet asymptotically converges to the principal subspace. In the rest of the section, we give a detailed description of our experimental setup to show the applicability of ManifoldNet to dimensionality reduction.

3.2.1 Implementation Details

A traditional convolutional autoencoder performs non-linear dimensionality reduction by learning an identity function through a small latent space. A common technique used when the desired latent space is smaller than the output of the encoder is to apply a fully connected layer to match dimensions. We replace this fully connected layer by a weighted subspace averaging and projection block, called the Grassmann averaging layer. Specifically, we compute the weighted

Fréchet Mean of the output of the encoder to get a subspace in the encoder output space. We then project the encoder output onto this space to obtain a reduced dimensionality latent space. We explicitly perform linear dimensionality reduction in the latent space, hence, we should expect the encoder to linearize the data manifold to some degree, followed by a linear dimensionality reduction from the Grassmann averaging layer. When this layer is used in a larger network we add a weight penalty to the loss function of the form $(\sum w_i - 1)^2$ to ensure that we compute a proper weighted Fréchet Mean. In general this offers a significant parameter reduction while also increasing the reconstruction error performance of the autoencoder and giving realistic reconstructions. We call an autoencoder with the Grassmann averaging block an autoencoder+iFME network, as shown in Fig. 3. In the experiments we compare this to other dimensionality reduction techniques, including regular autoencoders that use fully connected layers to match encoder and latent space dimensions. The PyTorch code used to run some of these experiments, including a PyTorch module for easily using a Grassmann averaging layer are accessible via GitHub ¹.

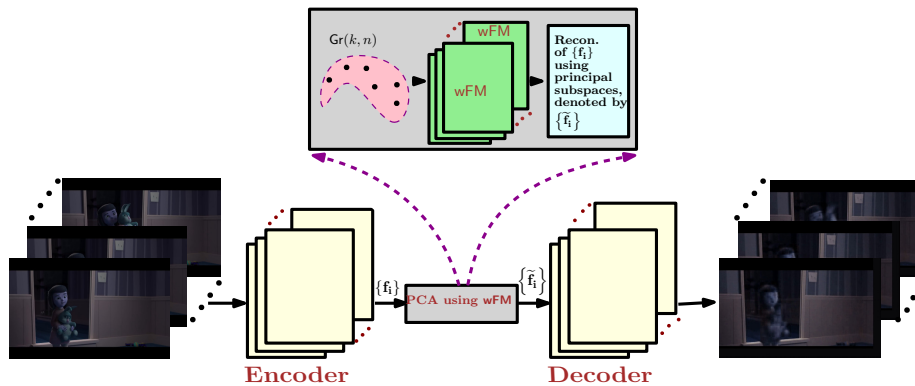


Figure 3: Schematic description of autoencoder+iFME network

3.2.2 Video Reconstruction Experiment

Assume we start with an $N \times 3 \times W \times H$ video, where N, W , and H are the number of frames, the frame width and the frame height respectively. Then, we apply an encoder in parallel to the frames to obtain a $N \times K \times M$ feature video F , where K and M are the channels and feature dimension, respectively. Finally, we compute the weighted FM of F as N vectors in \mathbf{R}^{KM} and project F onto this subspace to get a reduced dimensionality latent space. From here we proceed as in a regular autoencoder, backpropagating the L^2 reconstruction error throughout the network. Note that here we can interpret the Grassmann averaging layer weights as indicating the relative importance of different temporal segments of the video for the purpose of learning reconstructable features. To

¹<https://github.com/jjbouza/manifold-net>

compare with a regular autoencoder we simply remove the Grassmann averaging layer and replace it with a fully connected layer that maps to the same latent space dimension. This is justified by the fact that both operations are linear on the data, i.e. the Grassmann averaging block is not adding additional non-linear capacity to the network.

We begin by testing on a 1000 frame color sample of video from the 1964 film “Santa Clause Conquers the Martians” of frame size 320×240 . Here we use an 8 layer encoding-decoding architecture with **Conv** \rightarrow **ELU** \rightarrow **Batchnorm** layers, with the final layer applying a sigmoid activation to normalize pixel values.

The encoder returns a feature video consisting of 128 channels of size 120 for a dimension of 1000×15360 . We compare a fully connected layer to a Grassmann averaging layer, both mapping to a desired latent space of dimension 1000×20 . The per pixel average reconstruction error for the Grassmann block network is 0.0110, compared to 0.0122 for the fully connected network, representing an improvement of 10.9%. In general, the Grassmann averaging layer tends to do as well or better than the fully connected layer. Although in theory the fully connected layer can learn the same mapping as the Grassmann averaging layer, it has a much larger parameter space to search for this solution, implying that it is more likely to get trapped in local minima in the low loss regions of the loss surface. We also observe a parameter reduction of 46%, which can be attributed to the number of parameters in the large fully connected layer. In general the Grassmann averaging layer network is slower per iteration than the fully connected network, but also tends to exhibit faster convergence so that the time to reach the same reconstruction error is less for the Grassmann averaging layer. This is depicted in Fig. 4, where, computation time is plotted against error tolerance for the autoencoder and the iFME+autoencoder. Overall, we see an improvement in all major performance categories.

It is possible to obtain a low reconstruction error on autoencoding tasks and still observe low visual quality reconstructions. To ensure this is not the case we run the same experiment on 300 frames of the 1280×720 short film ², with a latent space frame dimension of 300×50 . In Fig. 5 we compare the visual quality of our autoencoder to that of PCA with 50 principal components, i.e., we reduce the dimension from $1280 \times 720 \times 3$ to 50. The entire sample reconstruction is shown in ³ (in the same order as in Fig. 5).

3.2.3 MNIST Reconstruction Experiment

Finally, we applied the ManifoldNet framework to MNIST data ⁴. We trained a 4-layer autoencoder on a random sample of 1000 images and test the reconstruction error on a 100 sample test set. Here the Grassmann averaging layer reduces from an encoder dimension of 25 to a latent space of dimension 2. In Fig. 7 we compared the reconstructions of our autoencoder+iFME to a regular autoencoder

²<https://www.youtube.com/watch?v=t1hMBnIMt5I>

³<https://streamable.com/3yqrx>

⁴<http://yann.lecun.com/exdb/mnist/>

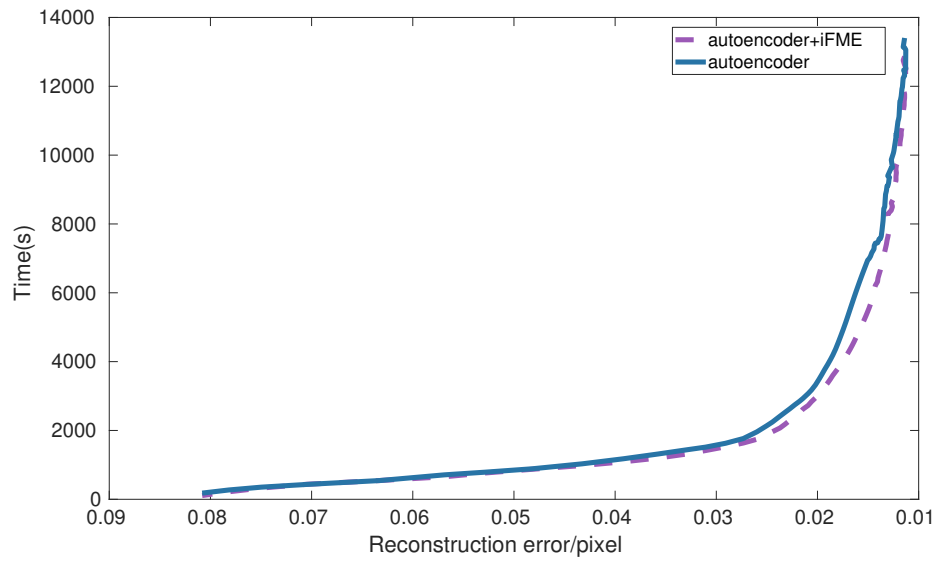


Figure 4: Computation time vs. error tolerance plot comparison between autoencoder and iFME+autoencoder

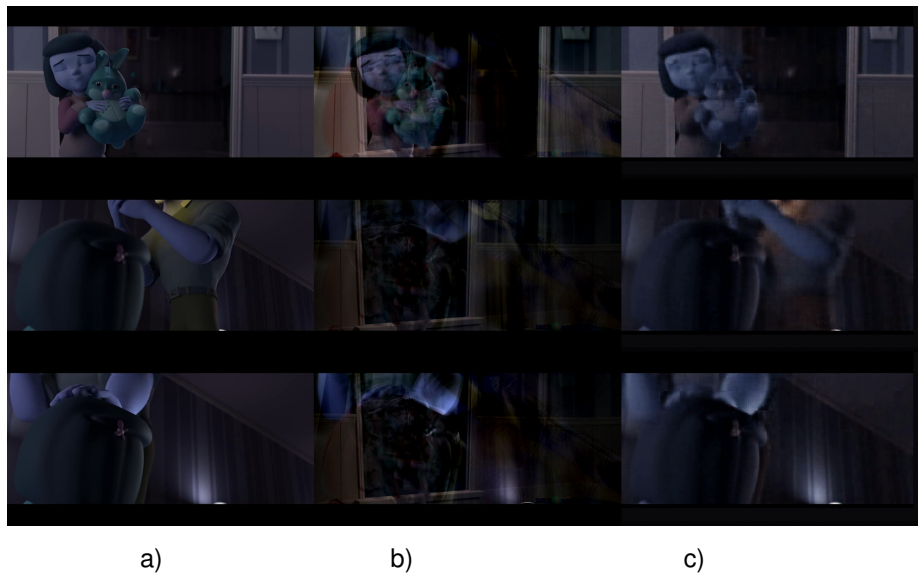


Figure 5: Reconstruction of select movie frames (a) original frame (b) using PCA (c) using iFME+autoencoder

with a fully connected layer after the encoder and to a PCA reconstruction in image space.

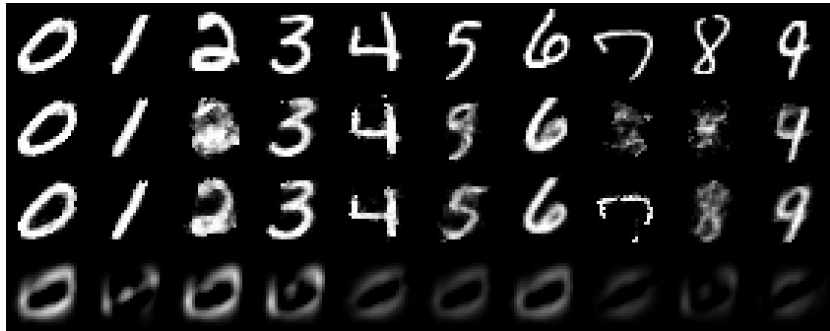


Figure 6: Reconstructions of (a), a sample of the validation set: (b) Regular autoencoder (c) Autoencoder+iFME (d) PCA

To evaluate the validation set reconstruction performance rigorously we trained a simple two layer fully connected classifier on the entire MNIST data set, achieving a training accuracy of 99.97% after 120 epochs of training. We then applied this classifier to all of the test set reconstructions given by the above methods, and evaluated the accuracy of the reconstructions by measuring the classification accuracy of the classifier. These results are summarized in Fig. 7.

We observe that a regular autoencoder yielded marginally better classification accuracy on the training set, but autoencoder+iFME gave a much larger improvement on the test set. Since the fully connected layer at the end of the regular autoencoder can learn a mapping identical to the projection in our Grassmann averaging layer, we conclude that our method acts as a regularizer here, preventing overfitting to the training set.

	Autoencoder	Autoencoder+iFME	PCA
Training Set	0.862	0.8540	0.2300
Validation Set	0.4000	0.4600	0.2600

Figure 7: Classification Accuracy of MNIST data Classifier on Reconstructed Data

4 Conclusions

In this paper, we presented a novel deep network called ManifoldNets suited for processing manifold-valued data sets. Manifold-valued data are commonly encountered in many computer vision and medical imaging applications. Examples of such data include but are not limited to directional data which reside on a sphere, covariance descriptors which reside on the manifold of symmetric positive matrices and others. Note that the input to ManifoldNets are manifold-valued

and not real or complex-valued functions defined on non-Euclidean domains. The key contributions of this work are: (i) A novel generalization of the CNN to the case when the input data are manifold-valued using purely intrinsic operations that are natural to the manifold on which the data reside. (ii) Convolution is achieved as a weighted FM operation and a theorem on the equivariance of the weighted FM to natural group operations admitted by the manifold. This equivariance allows us to share the learned weights within a layer of the ManifoldNet. (iii) An efficient recursive weighted FM estimator that is provably convergent. (iv) Experimental results demonstrating the efficacy of ManifoldNets for, (a) video classification and (b) principal component computation from videos and reconstruction.

References

- [1] Bijan Afsari. Riemannian L^p center of mass: Existence, uniqueness, and convexity. *Proceedings of the American Mathematical Society*, 139(02):655–655, 2011.
- [2] V Arsigny, P Fillard, X Pennec, and N Ayache. Log-Euclidean metrics for fast and simple calculus on diffusion tensors. *Magn. Reson. Med.*, 56:411–421, 2006.
- [3] Y. Bengio, A. Courville, and P. Vincent. Representation learning: A review and new perspectives. *IEEE Transactions on Pattern Analysis and Machine Intelligence*, 35(8):1798–1828, 2013.
- [4] Silvere Bonnabel. Stochastic gradient descent on Riemannian manifolds. *Automatic Control, IEEE Transactions on*, 58(9):2217–2229, 2013.
- [5] Michael M Bronstein, Joan Bruna, Yann LeCun, Arthur Szlam, and Pierre Vandergheynst. Geometric deep learning: going beyond euclidean data. *IEEE Signal Processing Magazine*, 34(4):18–42, 2017.
- [6] Joan Bruna and Stephane Mallat. Invariant scattering convolution networks. *IEEE Transactions on Pattern Analysis and Machine Intelligence*, 2013.
- [7] R. Chakraborty, S. Hauberg, and B. C. Vemuri. Intrinsic grassmann averages for online linear and robust subspace learning. *2017 IEEE Conference on Computer Vision and Pattern Recognition*, pages 801–809, 2017.
- [8] R. Chakraborty, C.-H. Yang, X. Zhen, M. Banerjee, D. Archer, D. Vaillancourt, V. Singh, and B. C. Vemuri. Statistical Recurrent Models on Manifold valued Data. *ArXiv e-prints*, May 2018.
- [9] Rudrasis Chakraborty, Monami Banerjee, and Baba C Vemuri. H-CNNs: Convolutional Neural Networks for Riemannian Homogeneous Spaces. *arXiv preprint arXiv:1805.05487*, 2018.
- [10] Isaac Chavel. *Riemannian geometry: a modern introduction*, volume 98. Cambridge university press, 2006.
- [11] Taco Cohen and Max Welling. Group equivariant convolutional networks. In *International conference on machine learning*, pages 2990–2999, 2016.
- [12] Taco S Cohen, Mario Geiger, Jonas Köhler, and Max Welling. Spherical CNNs. *arXiv preprint arXiv:1801.10130*, 2018.

- [13] Michaël Defferrard, Xavier Bresson, and Pierre Vandergheynst. Convolutional neural networks on graphs with fast localized spectral filtering. In *Advances in Neural Information Processing Systems*, pages 3844–3852, 2016.
- [14] Sander Dieleman, Kyle W. Willett, and Joni Dambre. Rotation-invariant convolutional neural networks for galaxy morphology prediction. *Monthly Notices of the Royal Astronomical Society*, 2015.
- [15] Manfredo P Do Carmo. *Riemannian geometry*. Springer, 1992.
- [16] David Steven Dummit and Richard M Foote. *Abstract algebra*, volume 3. Wiley Hoboken, 2004.
- [17] Carlos Esteves, Christine Allen-Blanchette, Xiaowei Zhou, and Kostas Daniilidis. Polar Transformer Networks. *arXiv preprint arXiv:1709.01889*, 2017.
- [18] Robert Gens. Deep Symmetry Networks. *Nips 2014*, 2014.
- [19] Alvina Goh, Christophe Lenglet, Paul M Thompson, and René Vidal. A non-parametric riemannian framework for processing high angular resolution diffusion images and its applications to odF-based morphometry. *NeuroImage*, 56(3):1181–1201, 2011.
- [20] David Groisser. Newton’s method, zeroes of vector fields, and the Riemannian center of mass. *Advances in Applied Mathematics*, 33(1):95–135, 2004.
- [21] S. Hauberg, A. Feragen, R. Enficiaud, and M. J. Black. Scalable robust principal component analysis using grassmann averages. *IEEE Transactions on Pattern Analysis and Machine Intelligence*, pages 2298–2311, 2016.
- [22] Mikael Henaff, Joan Bruna, and Yann LeCun. Deep convolutional networks on graph-structured data. *arXiv preprint arXiv:1506.05163*, 2015.
- [23] Sepp Hochreiter and Jürgen Schmidhuber. Long short-term memory. *Neural Comput.*, 9(8):1735–1780, November 1997.
- [24] Zhiwu Huang and Luc J Van Gool. A Riemannian Network for SPD Matrix Learning. In *AAAI*, volume 1, page 3, 2017.
- [25] Zhiwu Huang, Jiqing Wu, and Luc Van Gool. Building deep networks on Grassmann manifolds. *arXiv preprint arXiv:1611.05742*, 2016.
- [26] Max Jaderberg, Karen Simonyan, Andrew Zisserman, and Others. Spatial transformer networks. In *Advances in neural information processing systems*, pages 2017–2025, 2015.
- [27] Wilfrid S Kendall. Probability, convexity, and harmonic maps with small image. I. Uniqueness and finite existence. *Proc. London Math. Soc. (3)*, 61(2):371–406, 1990.
- [28] D. P. Kingma and P. Dhariwal. Glow: Generative Flow with Invertible 1x1 Convolutions. *ArXiv e-prints 1807.03039*, 2018.
- [29] D. P Kingma and M. Welling. Auto-Encoding Variational Bayes. *ArXiv e-prints 1312.6114*, 2013.
- [30] Risi Kondor and Shubhendu Trivedi. On the generalization of equivariance and convolution in neural networks to the action of compact groups. *arXiv preprint arXiv:1802.03690*, 2018.
- [31] Alex Krizhevsky, Ilya Sutskever, and Geoffrey E Hinton. ImageNet Classification with Deep Convolutional Neural Networks. *Advances In Neural Information Processing Systems*, 2012.

- [32] Yann LeCun, Léon Bottou, Yoshua Bengio, and Patrick Haffner. Gradient-based learning applied to document recognition. *Proceedings of the IEEE*, 1998.
- [33] Stéphane Mallat. Understanding Deep Convolutional Networks. *Philosophical Transactions A*, 374:20150203, 2016.
- [34] Jonathan H Manton. A globally convergent numerical algorithm for computing the centre of mass on compact lie groups. In *Control, Automation, Robotics and Vision Conference, 2004. ICARCV 2004 8th*, volume 3, pages 2211–2216. IEEE, 2004.
- [35] Jonathan Masci, Davide Boscaini, Michael Bronstein, and Pierre Vandergheynst. Geodesic convolutional neural networks on riemannian manifolds. In *Proceedings of the IEEE international conference on computer vision workshops*, pages 37–45, 2015.
- [36] Maurice Fréchet. Les éléments aléatoires de nature quelconque dans un espace distancié. *Annales de l'I. H. P.*, 10(4):215–310, 1948.
- [37] J. B. Oliva, B. Póczos, and J. Schneider. The Statistical Recurrent Unit. *ArXiv e-prints*, March 2017.
- [38] Aäron van den Oord, Nal Kalchbrenner, Oriol Vinyals, Lasse Espeholt, Alex Graves, and Koray Kavukcuoglu. Conditional image generation with pixelcnn decoders. *Proceedings of the 30th International Conference on Neural Information Processing Systems*, pages 4797–4805, 2016.
- [39] Edouard Oyallon and Stéphane Mallat. Deep roto-translation scattering for object classification. In *Proceedings of the IEEE Computer Society Conference on Computer Vision and Pattern Recognition*, 2015.
- [40] Siamak Ravanbakhsh, Jeff Schneider, and Barnabas Póczos. Equivariance through parameter-sharing. *arXiv preprint arXiv:1702.08389*, 2017.
- [41] Hesamoddin Salehian, Rudransh Chakraborty, Edward Ofori, David Vaillancourt, and Baba C Vemuri. An efficient recursive estimator of the Fréchet mean on a hypersphere with applications to Medical Image Analysis. *Mathematical Foundations of Computational Anatomy*, 2015.
- [42] Nitish Srivastava, Elman Mansimov, and Ruslan Salakhutdinov. Unsupervised learning of video representations using lstms. In *Proceedings of the 32Nd International Conference on International Conference on Machine Learning - Volume 37, ICML'15*, pages 843–852. JMLR.org, 2015.
- [43] Karl-Theodor Sturm. Probability measures on metric spaces of nonpositive curvature. *Contemporary mathematics*, 338:357–390, 2003.
- [44] Aäron Van Den Oord, Nal Kalchbrenner, and Koray Kavukcuoglu. Pixel recurrent neural networks. *Proceedings of the 33rd International Conference on International Conference on Machine Learning - Volume 48*, pages 1747–1756, 2016.
- [45] Pascal Vincent, Hugo Larochelle, Isabelle Lajoie, Yoshua Bengio, and Pierre-Antoine Manzagol. Stacked denoising autoencoders: Learning useful representations in a deep network with a local denoising criterion. *Journal of Machine Learning Research*, 11, December 2010.
- [46] Daniel E Worrall, Stephan J Garbin, Daniyar Turmukhambetov, and Gabriel J Brostow. Harmonic networks: Deep translation and rotation equivariance. In *Proc. IEEE Conf. on Computer Vision and Pattern Recognition (CVPR)*, volume 2, 2017.

- [47] Y. Yang, D. Krompass, and V. Tresp. Tensor-Train Recurrent Neural Networks for Video Classification. *ArXiv e-prints*, July 2017.
- [48] K. Yu and M. Salzmann. Second-order Convolutional Neural Networks. *ArXiv e-prints*, March 2017.